

Structural Control with Multi-Subnet Wireless Sensing Feedback: Experimental Validation of Time-Delayed Decentralized \mathcal{H}_∞ Control Design

Yang Wang^{*1} and Kincho H. Law²

¹ *School of Civil and Environmental Engineering, Georgia Institute of Technology, Atlanta, GA 30332, USA*

² *Department of Civil and Environmental Engineering, Stanford University, Stanford, CA 94305, USA*

¹ *yang.wang@ce.gatech.edu*, ² *law@stanford.edu*

ABSTRACT

This study investigates the feasibility of deploying wireless communication and embedded computing for structural control applications. A feedback structural control system involves a network of sensors and control devices. As control devices are becoming smaller, more cost effective and reliable, opportunities are now available to instrument a structure with large number of control devices. However, instrumenting a large scale centralized control system with cables can be time consuming, labor intensive, and difficult to maintain and reconfigure. This study explores decentralized feedback control using wireless sensors incorporated with a computational core and a signal generation module. Decentralized control architectures are designed to make control decisions based on data acquired from sensors located in the vicinity of a control device.

Specifically, this paper describes the experimental validation of a time-delayed decentralized structural control strategy that aims to minimize the \mathcal{H}_∞ norm of a closed-loop control system. The decentralized controller design employs a homotopy method that gradually transforms a centralized controller into

* Corresponding author: Yang Wang, 790 Atlantic Dr NW, Atlanta, GA 30332-0355, USA. Tel: +001(404)894-1851, Fax: +001 (404)894-2278. E-mail: yang.wang@ce.gatech.edu.

multiple decentralized controllers. Linear matrix inequality constraints are included in the homotopic transformation to ensure optimal control performance. The paper also describes our first implementation of a real-time wireless sensing and control system that achieves simultaneous communication within multiple wireless subnets. Different decentralized \mathcal{H}_∞ control architectures are implemented with a network of wireless sensing and control units instrumented on a six-story scaled steel frame structure controlled by magnetorheological dampers. Shake table experiments are conducted to demonstrate the performance of the wireless decentralized control architectures.

Keywords: structural control, wireless sensing, feedback time delay, decentralized control, H-infinity control, homotopy method, linear matrix inequality.

1. INTRODUCTION

Utilizing a network of sensors, controllers and control devices, feedback control systems can potentially mitigate excessive dynamic responses of a structure subjected to strong dynamic loads, such as earthquakes or typhoons (Housner, *et al.* 1997). For a large scale structure, the instrumentation of a cable-based communication network that connects a large number of sensors, control devices, and controllers can be quite costly. As the size of the structure increases, the cost of installing the cables also grows in a rapid rate. Furthermore, maintaining the reliability and performance of a large-scale interconnected real-time system can be challenging; reconfiguring the system would require laborious rerouting of the cables. With the increasing availability of wireless communication and embedded computing technologies, there has been extensive work towards the development of wireless sensing technologies for structural monitoring applications (Straser and Kiremidjian 1998, Lynch, *et al.* 2006). The adoption of wireless sensing technologies can remedy the high installation expense of commercial cable-based systems, which can cost up to a few thousand dollars per sensing channel (Çelebi 2002). A natural extension of the wireless sensing technology, as it matures, is to explore its applicability for semi-active or active control by eradicating lengthy cables associated with traditional control systems. As the

building block of a wireless feedback control system, a wireless sensing and control unit can not only collect and communicate sensor data, but also make optimal control decisions and directly command control devices in real-time. This study further investigates the feasibility of deploying decentralized control algorithms that are performed over a wireless sensing and control network.

As control devices are becoming smaller, more cost effective and reliable, opportunities are now available to instrument a structure with large number of control devices (Spencer and Nagarajaiah 2003). With high density of sensing and control devices, scalability of control systems will be hindered by their dependence on centralized control strategies, where a central controller is responsible for acquiring data and making control decisions. To mitigate some of the difficulties with centralized feedback control systems, decentralized control strategies can be explored (Sandell, *et al.* 1978, Siljak 1991, Lunze 1992). Decentralized structural control systems exist; for example, the 170m-tall Shiodome Tower in Tokyo, Japan consists of 88 fully decentralized semi-active hydraulic (SHD) dampers (Kurino, *et al.* 2003, Shimizu, *et al.* 2004). However, for such a fully decentralized system, real-time control decision is made for each SHD damper, based upon the data of a stroke sensor and a load cell associated with this SHD damper alone. Our research focuses on decentralized control architectures that are designed to make decisions based on data acquired from a distributed network of sensors located in the vicinity of a control device. Decentralized feedback control can take advantage of a network of wireless sensors incorporated with a computational core and signal generation module (Wang, *et al.* 2007, Wang, *et al.* 2008). Embedded in the wireless sensing units, decentralized control algorithms can be performed in a parallel and distributive manner.

This paper describes the experimental study of a time-delayed decentralized structural control strategy that aims to minimize the \mathcal{H}_∞ norm of a closed-loop control system. \mathcal{H}_∞ control can offer excellent control performance particularly when “worst-case” external disturbances are encountered (Zhou, *et al.* 1996). Centralized \mathcal{H}_∞ controller design in the continuous-time domain for structural control has been studied by

many researchers (Johnson, *et al.* 1998, Mahmoud, *et al.* 1998, Wang 2003, Yang, *et al.* 2004, Balandin and Kogan 2005, Lin, *et al.* 2006). Their studies have shown the effectiveness of centralized \mathcal{H}_∞ control for civil structures. For example, it has been shown that \mathcal{H}_∞ control design can achieve excellent performance in attenuating transient vibrations of structures (Chase, *et al.* 1996). We have conducted numerical simulations to evaluate the performance of time delayed decentralized \mathcal{H}_∞ control (Wang, *et al.* 2009, Wang 2009). The decentralized controller design employs a homotopy method that gradually transforms a centralized controller into multiple decentralized controllers. Linear matrix inequality constraints are included in the homotopic transformation to ensure optimal control performance. It should be noted that homotopy approaches for decentralized \mathcal{H}_∞ control have also been explored by other researchers (Mehendale and Grigoriadis 2008). Our approach adapts the homotopy method described by Zhai, *et al.* (2001). The method was originally developed for designing decentralized \mathcal{H}_∞ controllers in continuous-time domain. Specifically, this paper presents an experimental study of the time-delayed decentralized \mathcal{H}_∞ controller design, implemented on a network of wireless sensing and control units.

In order to allow multiple decentralized controllers to simultaneously obtain real-time data from neighborhood sensors over a wireless network, multiple subnets that operate on different wireless communication channels are needed to minimize interference among the wireless units. Besides handling real-time communication, the microprocessor of each wireless sensing and control unit also needs to coordinate the sensing and actuation tasks (such as sensor interrogation, embedded computing, and control signal generation) with accurate timing. This paper presents the implementation of a real-time wireless feedback structural control system with multi-channel low-latency communication, utilizing the Narada wireless sensing and control unit designed by Swartz and Lynch (Swartz, *et al.* 2005, Swartz and Lynch 2009). Different decentralized \mathcal{H}_∞ control architectures are implemented with a network of wireless sensing and control units instrumented on a six-story steel frame structure. Semi-active

magnetorheological dampers are installed on the structure as control devices. Shake table experiments were conducted at the National Center for Research on Earthquake Engineering in Taiwan to examine the performance of different decentralized control architectures.

The paper is organized as follows. First, the formulation for decentralized \mathcal{H}_∞ controller design is summarized. The experimental setup of the six-story steel frame structure instrumented with wireless sensing and control system is then described. Details are provided on the control system architectures that achieve simultaneous real-time sensing feedback using multiple wireless subnets. Experimental results are presented to evaluate the effectiveness of the wireless decentralized \mathcal{H}_∞ control strategies. Finally, this paper is concluded with a brief summary and discussion.

2. OVERVIEW OF THE DECENTRALIZED STRUCTURAL CONTROL FORMULATION

2.1. Structural Control Formulation with Feedback Time Delay and Sensor Noise

For a structural model with n degrees-of-freedom (DOF) and instrumented with n_u control devices, the state-space representation of the discrete-time system can be written as (Wang, *et al.* 2009, Wang 2009):

$$\begin{cases} \mathbf{x}_S[k+1] = \mathbf{A}_d \mathbf{x}_S[k] + \mathbf{E}_d \mathbf{w}_1[k] + \mathbf{B}_d \mathbf{u}[k] \\ \mathbf{z}[k] = \mathbf{C}_z \mathbf{x}_S[k] + \mathbf{F}_z \mathbf{w}_1[k] + \mathbf{D}_z \mathbf{u}[k] \\ \mathbf{m}[k] = \mathbf{C}_m \mathbf{x}_S[k] + \mathbf{F}_m \mathbf{w}_1[k] + \mathbf{D}_m \mathbf{u}[k] \end{cases} \quad (1)$$

In Eqn (1), $\mathbf{x}_S[k] \in \mathbb{R}^{2n \times 1}$, $\mathbf{w}_1[k] \in \mathbb{R}^{n_w \times 1}$ and $\mathbf{u}[k] \in \mathbb{R}^{n_u \times 1}$ denote the state vector, the external excitation vector, and control force vector, respectively. For a lumped mass structural model with n floors, the state vector, \mathbf{x}_S , consists of the relative displacement q_i and relative velocity \dot{q}_i (with respect to the ground) for each floor i , $i = 1, \dots, n$.

$$\mathbf{x}_S = [q_1 \quad \dot{q}_1 \quad q_2 \quad \dot{q}_2 \quad \dots \quad q_n \quad \dot{q}_n]^T \quad (2)$$

where the superscript “T” represents vector or matrix transpose. Note that for the decentralized controller design, the relative displacement and relative velocity in the state vector \mathbf{x}_S are grouped by floor. The matrices $\mathbf{A}_d \in \mathbb{R}^{2n \times 2n}$, $\mathbf{E}_d \in \mathbb{R}^{2n \times n_{w1}}$, and $\mathbf{B}_d \in \mathbb{R}^{2n \times n_u}$ are, respectively, the discrete-time dynamics, excitation influence, and control influence matrices. The vectors, $\mathbf{z}[k] \in \mathbb{R}^{n_c \times 1}$ and $\mathbf{m}[k] \in \mathbb{R}^{n_m \times 1}$ represent, respectively, the response output (to be controlled using the feedback loop) and the sensor measurement vector. Correspondingly, the matrices \mathbf{C}_z , \mathbf{F}_z , and \mathbf{D}_z are termed the output parameter matrices, and the matrices \mathbf{C}_m , \mathbf{F}_m , and \mathbf{D}_m are the measurement parameter matrices. The dimensions of these parameter matrices should be compatible with corresponding vectors in Eqn (1).

Suppose time delay over one sampling period ΔT exists for the sensor measurement signal $\mathbf{m}[k]$ in the feedback process, for example, due to computational and/or communication overhead. Taking into consideration of sensor noise, denoted as $\mathbf{w}_2[k] \in \mathbb{R}^{n_{w2} \times 1}$, a discrete-time system can be defined as:

$$\begin{cases} \mathbf{x}_{TD}[k+1] = \mathbf{A}_{TD} \mathbf{x}_{TD}[k] + \mathbf{B}_{TD} \begin{bmatrix} \mathbf{m}[k] \\ \mathbf{w}_2[k] \end{bmatrix} \\ \mathbf{y}[k] = \mathbf{C}_{TD} \mathbf{x}_{TD}[k] + \mathbf{D}_{TD} \begin{bmatrix} \mathbf{m}[k] \\ \mathbf{w}_2[k] \end{bmatrix} \end{cases} \quad (3)$$

Here, we let $\mathbf{A}_{TD} = \mathbf{0}$, $\mathbf{B}_{TD} = [\mathbf{I} \quad \mathbf{0}]$, $\mathbf{C}_{TD} = \mathbf{I}$, and $\mathbf{D}_{TD} = [\mathbf{0} \quad s_{w_2} \mathbf{I}]$ (where \mathbf{I} represents an identity matrix with compatible dimension). The inputs to the time-delay system are the measurement signal $\mathbf{m}[k]$ and the sensor noise $\mathbf{w}_2[k] \in \mathbb{R}^{n_{w2} \times 1}$. The output of the time-delay system is the delayed noisy signal $\mathbf{y}[k] \in \mathbb{R}^{n_y \times 1}$, which is the feedback signal to be used for control decisions. Using this formulation, the three vectors, including the measurement signal $\mathbf{m}[k]$, the sensor noise $\mathbf{w}_2[k]$, and the delayed noisy signal $\mathbf{y}[k]$, have the

same dimensions. In addition, the dimension of the state vector $\mathbf{x}_{TD}[k] \in \mathbb{R}^{n_{TD} \times 1}$ of system defined in Eqn (3) is also the same, i.e.

$$n_{TD} = n_m = n_{w2} = n_y \quad (4)$$

The parameter s_{w2} is a scaling factor representing sensor noise level. For simplicity, we assume the same scaling factor applies to all sensors, although, in general, different scaling factors can be assigned to different sensors by modifying the diagonal entries in the matrix $s_{w2}\mathbf{I}$. It should be noted that the formulation can also be extended to model multiple time delay steps, as well as different time delays for different sensors.

The dynamical system described by Eqn (1) and the time-delay system described in Eqn (3) are connected to constitute an open-loop system depicted in Figure 1. Since the sensor measurement vector $\mathbf{m}[k]$ is both the output from the structural system and the input to the time-delay system, $\mathbf{m}[k]$ becomes an internal variable of the open-loop system. The inputs to the open-loop system include the excitation $\mathbf{w}_1[k]$, the sensor noises $\mathbf{w}_2[k]$, and the control forces $\mathbf{u}[k]$, while the outputs include the structural responses $\mathbf{z}[k]$ and the feedback signals $\mathbf{y}[k]$. The number of state variables in the open-loop system is thus equal to the total number of state variables in the structural system and the time-delay system:

$$n_{OL} = 2n + n_{TD} \quad (5)$$

Cascading the structural system and the time-delay system (for example, using the `sysic` command in the Matlab Robust Control Toolbox (Chiang and Safonov 1998)), the complete open-loop system is denoted as follows:

$$\begin{cases} \mathbf{x}[k+1] = \mathbf{A}\mathbf{x}[k] + \mathbf{B}_1\mathbf{w}[k] + \mathbf{B}_2\mathbf{u}[k] \\ \mathbf{z}[k] = \mathbf{C}_1\mathbf{x}[k] + \mathbf{D}_{11}\mathbf{w}[k] + \mathbf{D}_{12}\mathbf{u}[k] \\ \mathbf{y}[k] = \mathbf{C}_2\mathbf{x}[k] + \mathbf{D}_{21}\mathbf{w}[k] + \mathbf{D}_{22}\mathbf{u}[k] \end{cases} \quad (6)$$

where $\mathbf{w} = [\mathbf{w}_1^T \ \mathbf{w}_2^T]^T \in \mathbb{R}^{n_w \times 1}$ contains both the external excitation \mathbf{w}_1 and the sensor noise \mathbf{w}_2 .

For feedback control, the controller system takes the signal $\mathbf{y}[k]$ as input, and outputs the desired (optimal) control force vector $\mathbf{u}[k]$ according to the state-space formulation for the dynamic controller:

$$\begin{cases} \mathbf{x}_G[k+1] = \mathbf{A}_G\mathbf{x}_G[k] + \mathbf{B}_G\mathbf{y}[k] \\ \mathbf{u}[k] = \mathbf{C}_G\mathbf{x}_G[k] + \mathbf{D}_G\mathbf{y}[k] \end{cases} \quad (7)$$

where \mathbf{A}_G , \mathbf{B}_G , \mathbf{C}_G and \mathbf{D}_G are the parametric matrices of the controller to be computed and, for convenience, are often collectively denoted by a controller matrix $\mathbf{G} \in \mathbb{R}^{(n_G+n_u) \times (n_G+n_y)}$ as:

$$\mathbf{G} = \begin{bmatrix} \mathbf{A}_G & \mathbf{B}_G \\ \mathbf{C}_G & \mathbf{D}_G \end{bmatrix} \quad (8)$$

In this study, we assume both the controller and the open-loop system have the same number of state variables, i.e. $\mathbf{A}_G \in \mathbb{R}^{n_G \times n_G}$ and $n_G = n_{OL}$ (Eqn (5)).

2.2. Decentralized Control Formulation

A decentralized control strategy can be defined by specifying a sparsity pattern in the controller matrices \mathbf{A}_G , \mathbf{B}_G , \mathbf{C}_G and \mathbf{D}_G . The feedback signals $\mathbf{y}[k]$ and the control forces $\mathbf{u}[k]$ are divided into N groups. For each group of control forces, the feedback signals corresponding to the communication patterns are grouped accordingly to reflect the decentralized control decisions. The decentralized architecture, denoted

by a set of controllers \mathbf{G}_I , \mathbf{G}_{II} , ..., and \mathbf{G}_N , can be obtained by specifying that the controller matrices in Eqn (8) have block diagonal forms:

$$\mathbf{A}_G = \text{diag}(\mathbf{A}_{G_I}, \mathbf{A}_{G_{II}}, \dots, \mathbf{A}_{G_N}) \quad (9a)$$

$$\mathbf{B}_G = \text{diag}(\mathbf{B}_{G_I}, \mathbf{B}_{G_{II}}, \dots, \mathbf{B}_{G_N}) \quad (9b)$$

$$\mathbf{C}_G = \text{diag}(\mathbf{C}_{G_I}, \mathbf{C}_{G_{II}}, \dots, \mathbf{C}_{G_N}) \quad (9c)$$

$$\mathbf{D}_G = \text{diag}(\mathbf{D}_{G_I}, \mathbf{D}_{G_{II}}, \dots, \mathbf{D}_{G_N}) \quad (9d)$$

The control system in Eqn (7) is thus equivalent to a set of uncoupled decentralized control subsystems, each requiring only one group of feedback signals to determine the desired (optimal) control forces for that subsystem i ($i = I, II, \dots, N$).

$$\begin{cases} \mathbf{x}_{G_i}[k+1] = \mathbf{A}_{G_i} \mathbf{x}_{G_i}[k] + \mathbf{B}_{G_i} \mathbf{y}_i[k] \\ \mathbf{u}_i[k] = \mathbf{C}_{G_i} \mathbf{x}_{G_i}[k] + \mathbf{D}_{G_i} \mathbf{y}_i[k] \end{cases} \quad (10a)$$

$$\quad (10b)$$

Assuming that the \mathbf{D}_{22} matrix in the open-loop system in Eqn (6) is a zero matrix, the following notations have been defined by Zhai, *et al.* (2001):

$$\begin{bmatrix} \tilde{\mathbf{A}} & \tilde{\mathbf{B}}_1 & \tilde{\mathbf{B}}_2 \\ \tilde{\mathbf{C}}_1 & \tilde{\mathbf{D}}_{11} & \tilde{\mathbf{D}}_{12} \\ \tilde{\mathbf{C}}_2 & \tilde{\mathbf{D}}_{21} & \tilde{\mathbf{D}}_{22} \end{bmatrix} = \begin{bmatrix} \mathbf{A} & \mathbf{0} & \mathbf{B}_1 & \mathbf{0} & \mathbf{B}_2 \\ \mathbf{0} & \mathbf{0}_{n_G} & \mathbf{0} & \mathbf{I}_{n_G} & \mathbf{0} \\ \mathbf{C}_1 & \mathbf{0} & \mathbf{D}_{11} & \mathbf{0} & \mathbf{D}_{12} \\ \mathbf{0} & \mathbf{I}_{n_G} & \mathbf{0} & & \\ \mathbf{C}_2 & \mathbf{0} & \mathbf{D}_{21} & & \end{bmatrix} \quad (11)$$

Using the definitions above, the closed-loop system in Figure 1 can be formulated by concatenating the open-loop system with the controller system:

$$\begin{cases} \mathbf{x}_{CL}[k+1] = \mathbf{A}_{CL}\mathbf{x}_{CL}[k] + \mathbf{B}_{CL}\mathbf{w}[k] \\ \mathbf{z}[k] = \mathbf{C}_{CL}\mathbf{x}_{CL}[k] + \mathbf{D}_{CL}\mathbf{w}[k] \end{cases} \quad (12)$$

where

$$\mathbf{A}_{CL} = \tilde{\mathbf{A}} + \tilde{\mathbf{B}}_2 \mathbf{G} \tilde{\mathbf{C}}_2 \quad (13a)$$

$$\mathbf{B}_{CL} = \tilde{\mathbf{B}}_1 + \tilde{\mathbf{B}}_2 \mathbf{G} \tilde{\mathbf{D}}_{21} \quad (13b)$$

$$\mathbf{C}_{CL} = \tilde{\mathbf{C}}_1 + \tilde{\mathbf{D}}_{12} \mathbf{G} \tilde{\mathbf{C}}_2 \quad (13c)$$

$$\mathbf{D}_{CL} = \tilde{\mathbf{D}}_{11} + \tilde{\mathbf{D}}_{12} \mathbf{G} \tilde{\mathbf{D}}_{21} \quad (13d)$$

and \mathbf{G} is defined in Eqn (8). Note that the input $\mathbf{w}[k]$ to the closed-loop system includes both the external excitation \mathbf{w}_1 and sensor noise \mathbf{w}_2 , and the output $\mathbf{z}[k]$ is the structural response.

A decentralized \mathcal{H}_∞ structural control design using a homotopy method with linear matrix inequality (LMI) constraints is adopted in this study. Let $\mathbf{H}_{\mathbf{z}\mathbf{w}} \in \mathbb{C}^{n_z \times n_w}$ represent the discrete-time closed-loop transfer function from the disturbance \mathbf{w} to the output response \mathbf{z} . The objective of \mathcal{H}_∞ control is to minimize the \mathcal{H}_∞ -norm of the closed-loop system:

$$\|\mathbf{H}_{\mathbf{z}\mathbf{w}}\|_\infty = \sup_{\omega \in [-\omega_N, \omega_N]} \bar{\sigma}[\mathbf{H}_{\mathbf{z}\mathbf{w}}(e^{j\omega\Delta T})] \quad (14)$$

where ω represents angular frequency, ΔT is the sampling period, $\omega_N = \pi/\Delta T$ is the Nyquist frequency, j is the imaginary unit, and $\bar{\sigma}[\cdot]$ denotes the largest singular value of a matrix. In essence, the \mathcal{H}_∞ -norm represents the largest amplification gain from the disturbance \mathbf{w} to the output \mathbf{z} within the Nyquist frequency range.

Following the Bounded Real Lemma, the performance criterion $\|\mathbf{H}_{zw}\|_\infty < \gamma$ can be restated using a matrix variable \mathbf{F} which is a function of \mathbf{G} and \mathbf{P} as (Gahinet and Apkarian 1994):

$$\mathbf{F}(\mathbf{G}, \mathbf{P}) = \begin{bmatrix} -\mathbf{P} & \mathbf{P}(\tilde{\mathbf{A}} + \tilde{\mathbf{B}}_2 \mathbf{G} \tilde{\mathbf{C}}_2) & \mathbf{P}(\tilde{\mathbf{B}}_1 + \tilde{\mathbf{B}}_2 \mathbf{G} \tilde{\mathbf{D}}_{21}) & \mathbf{0} \\ * & -\mathbf{P} & \mathbf{0} & (\tilde{\mathbf{C}}_1 + \tilde{\mathbf{D}}_{12} \mathbf{G} \tilde{\mathbf{C}}_2)^T \\ * & * & -\gamma \mathbf{I} & (\tilde{\mathbf{D}}_{11} + \tilde{\mathbf{D}}_{12} \mathbf{G} \tilde{\mathbf{D}}_{21})^T \\ * & * & * & -\gamma \mathbf{I} \end{bmatrix} < 0 \quad (15)$$

That is, if there exists a decentralized controller \mathbf{G} (with parameter structures illustrated in Eqn (9)), a positive real number γ and a symmetric positive definite matrix \mathbf{P} , such that $\mathbf{F}(\mathbf{G}, \mathbf{P}) < 0$, then the closed-loop \mathcal{H}_∞ -norm is less than γ . Because both \mathbf{G} and \mathbf{P} are unknown variables, the optimization problem has a bilinear matrix inequality (BMI) constraint (VanAntwerp and Braatz 2000). When there is no sparsity requirement on the matrix \mathbf{G} , efficient solvers that minimize the closed-loop \mathcal{H}_∞ -norm are available for computing an ordinary (i.e. a centralized) controller matrix \mathbf{G}_C (Gahinet and Apkarian 1994, Chiang and Safonov 1998):

$$\mathbf{G}_C = \begin{bmatrix} \mathbf{A}_{G_C} & \mathbf{B}_{G_C} \\ \mathbf{C}_{G_C} & \mathbf{D}_{G_C} \end{bmatrix} \quad (16)$$

For decentralized control where the information feedback are specified by the sparsity patterns in the controller matrices, however, off-the-shelf algorithms for solving the optimization problem with BMI constraints are not available (VanAntwerp and Braatz 2000). In this study, the homotopy method described by Zhai, *et al.* (2001) originally developed for designing decentralized \mathcal{H}_∞ controllers in continuous-time domain is adapted for the discrete-time feedback control problem.

Starting with a centralized controller, the algorithm searches for a decentralized controller along following homotopy path:

$$\mathbf{G} = (1 - \lambda)\mathbf{G}_C + \lambda\mathbf{G}_D, 0 \leq \lambda \leq 1 \quad (17)$$

where λ gradually increases from 0 to 1. \mathbf{G}_C represents the initial centralized controller shown in Eqn (16), and \mathbf{G}_D represents the desired decentralized controller with a specified sparsity pattern shown in Eqn (9). In this way, the BMI constraint in Eqn (15) degenerates into a linear matrix inequality (LMI) constraint. For convenience, a matrix variable \mathbf{H} is defined based on Eqn (15) as a function of variables \mathbf{G}_D , \mathbf{P} , and λ :

$$\mathbf{H}(\mathbf{G}_D, \mathbf{P}, \lambda) = \mathbf{F}(\mathbf{G}, \mathbf{P}) = \mathbf{F}((1 - \lambda)\mathbf{G}_C + \lambda\mathbf{G}_D, \mathbf{P}) < 0 \quad (18)$$

Note that the centralized controller \mathbf{G}_C is initially solved using any conventional methods and is kept constant during the homotopy search. The method gradually transforms a centralized controller into a set of uncoupled decentralized controllers corresponding to certain decentralized feedback patterns. At each homotopy step, LMI constraints are used to ensure the closed-loop \mathcal{H}_∞ norm performance. Details on the homotopy method for the discrete-time delay decentralized control problem have been described elsewhere (Wang, *et al.* 2009, Wang 2009).

3. SHAKE-TABLE EXPERIMENTS WITH A SIX-STORY LABORATORY STRUCTURE

To study the performance of the decentralized \mathcal{H}_∞ structural control architecture with a wireless feedback control system, shake table experiments on a six-story scaled structure were conducted at the National

Center for Research on Earthquake Engineering (NCREE) in Taipei, Taiwan. This section describes the wireless feedback control system, experimental setup, control formulation, and test results.

3.1. Experimental Setup for Decentralized Wireless Feedback Control

A laboratory six-story steel frame structure, instrumented with RD-1005-3 magnetorheological (MR) dampers manufactured by Lord Corporation, is designed and constructed by researchers at NCREE (see Figure 2a). The structure is mounted on a 5m × 5m six-DOF shake table, which can generate ground excitations with frequencies spanning from 0.1Hz to 50Hz. For this study, only longitudinal excitations are used. Accelerometers, velocity meters, and linear variable displacement transducers (LVDT) are instrumented on the shake table and on every floor to measure the dynamic responses of the structure. The sensors are interfaced to a high-precision cabled data acquisition (DAQ) system at the NCREE facility; the cabled DAQ system is set to operate with a sampling rate of 200 Hz.

For wireless sensing and control, the prototype Narada wireless unit (Swartz, *et al.* 2005, Swartz and Lynch 2009) developed at the University of Michigan is employed. As shown in Figure 3, each Narada unit consists of four functional modules: computational core, sensor signal digitization, wireless communication, and control signal generation. The computational core is a low-power 8-bit Atmel ATmega128 microcontroller. An external Static Random Access Memory (SRAM) of 128kB is integrated with the computational core to extend data storage and to facilitate data interrogation. The sensor signal digitization module, which mainly consists of the Texas Instrument 16-bit A/D converter ADS8341, converts analog sensor signals into digital data. Up to four analog sensors can be connected with each Narada unit. Sensor data is transferred to the ATmega128 microcontroller through a high-speed Serial Peripheral Interface (SPI) port. Application programs are embedded and executed by the microcontroller. Analog signals as control commands are sent to structural control devices through the Texas Instruments D/A converter DAC7612. Up to two structural control devices can be commanded by one Narada unit. The wireless unit communicates with other units or a computer server through the Chipcon CC2420 wireless modem. Onboard communication between the CC2420 modem and the ATmega128

microcontroller is also through the SPI port. With the Chipcon CC2420 wireless modem incorporated in the Narada units, the transmission of a 10-byte packet takes only about 1.5~2 ms. Low-latency wireless transmission is particularly beneficial for feedback structural control applications, because low communication latency leads to high sampling frequency and low feedback delay.

The basic configuration of the wireless sensing and control system for the 6-story structure is schematically shown in Figure 2(b). A total of six Narada wireless units are installed in accordance with the deployment strategy. In the experiments, each Narada wireless unit collects velocity data at its own floor as well as the floor above from the Tokyo Sokushin VSE15-D velocity meters that provide absolute velocity measurements. The sensitivity of the velocity meter is 10V/(m/s) with a measurement limit of ± 1 m/s. A remote data and command server with a wireless transceiver is also included for initiating each test run, and for retrieving test data from the six wireless units.

In addition to collecting and transmitting the velocity data, each wireless unit sends command signal to the MR damper that it is connected to. The damper on each floor is connected to the upper floor through a V-brace (Figure 2a). Each damper can provide a maximum damping force over 2kN. The damping properties can be changed by the command voltage signal (ranging from 0 to 0.8V) through an input current source, which determines the electric current of the electromagnetic coil in the MR damper. The current then generates a variable magnetic field that sets the viscous damping properties of the MR damper. Calibration tests are first conducted on the MR dampers before mounting them onto the structure and a modified Bouc-Wen force-displacement model is developed for the damper (Lu, *et al.* 2008). In the feedback control tests, the hysteresis model parameters for the MR dampers are an integral element of the control procedure embedded in the wireless units for calculating command voltages for the dampers.

3.2. Formulation for the Controller Design

For the experimental setup, the velocity differences between every two neighboring floors are obtained by the wireless units as the sensor measurements $\mathbf{m}[k]$ in Eqn (1):

$$\mathbf{m} = [\dot{q}_1 \quad \dot{q}_2 - \dot{q}_1 \quad \cdots \quad \dot{q}_n - \dot{q}_{n-1}]^T \quad (19)$$

With the state vector defined in Eqn (2), the associated measurement matrices are chosen as:

$$[\mathbf{C}_m]_{n \times 2n}(i, j) = \begin{cases} 1 & \text{if } j = 2i \\ -1 & \text{if } j = 2i - 2 \\ 0 & \text{otherwise} \end{cases} \quad (20a)$$

$$\mathbf{F}_m = \mathbf{0} \quad (20b)$$

$$\mathbf{D}_m = \mathbf{0} \quad (20c)$$

When formulating the \mathcal{H}_∞ controllers, inter-story drifts are considered as the major controlling factors for minimizing the dynamic responses. Accordingly, the output matrices are defined as:

$$\mathbf{C}_z = \begin{bmatrix} \mathbf{C}_{z_1} \\ \mathbf{0}_{n \times 2n} \end{bmatrix} \text{ where } [\mathbf{C}_{z_1}]_{n \times 2n}(i, j) = \begin{cases} \sqrt{300} & \text{if } j = 2i - 1 \\ -\sqrt{300} & \text{if } j = 2i - 3 \\ 0 & \text{otherwise} \end{cases} \quad (21a)$$

$$\mathbf{F}_z = \mathbf{0} \quad (21b)$$

$$\mathbf{D}_z = \begin{bmatrix} \mathbf{0}_{n \times n} \\ \mathbf{I}_{n \times n} \end{bmatrix} \times 10^{-4.5} \quad (21c)$$

The assignments for \mathbf{C}_z , \mathbf{F}_z , and \mathbf{D}_z result in an output vector $\mathbf{z}[k] \in \mathbb{R}^{2n \times 1}$ whose 2-norm is a quadratic function of the inter-story drifts and the control forces:

$$\begin{aligned} \|\mathbf{z}[k]\|_2^2 &= \|\mathbf{C}_z \mathbf{x}_s[k] + \mathbf{D}_z \mathbf{u}[k]\|_2^2 \\ &= 300 \sum_{i=1}^n (q_i[k] - q_{i-1}[k])^2 + 10^{-9} \sum_{i=1}^n u_i^2[k] \end{aligned} \quad (22a)$$

Where $q_0[k]$ represents ground displacement, and $q_i[k]$ ($i = 1 \dots n$) represents floor displacement relative to the ground (which means that $q_i[k] - q_{i-1}[k]$ for $i = 2 \dots n$ represents inter-story drift); $u_i[k]$ represents control force provided by control device between every two neighboring floors. The \mathcal{H}_∞ controller design aims to minimize the closed-loop \mathcal{H}_∞ -norm, which is defined as the system norm from the excitation input to the output $\mathbf{z}[k]$. The relative balancing between the structural response and the control effort is reflected by the magnitude of the output matrices, \mathbf{C}_z and \mathbf{D}_z . If higher attenuation of structural response is needed, larger magnitude should be assigned to \mathbf{C}_z ; on the contrary, if less control effort is available, larger magnitude should be assigned to \mathbf{D}_z .

Four decentralized/centralized feedback control architectures are adopted in the control experiments (Figure 4). The degrees of centralization (DC) of different architectures reflect the different communication network configurations, with each wireless channel representing one communication subnet. The wireless units assigned to a subnet are allowed to access the wireless sensor data within that subnet. As an example, for case DC2, each wireless channel covers only two stories and a total of three wireless channels (subnets) are in operation. For case DC1, each wireless unit only utilizes the velocity difference between two neighboring floors for control decisions; therefore, no wireless transmission is required. For case DC4, one wireless channel (subnet) is shared by all six wireless units, which is equivalent to a centralized feedback pattern.

Consider the decentralized case DC2 as an example, three uncoupled decentralized controllers are designed using the homotopy method (Wang, *et al.* 2009, Wang 2009). The dimensions of the three decentralized controllers are summarized in Table 1. Specifically, the two input variables to decentralized controller \mathbf{G}_I correspond to two inter-story velocities, $v_1 - v_0$ and $v_2 - v_1$, while the two input variables for \mathbf{G}_{II} correspond to $v_4 - v_3$ and $v_3 - v_2$; and so on. For case DC2, the two output variables of the decentralized controller \mathbf{G}_I (u_1 and u_2) are the desired optimal control forces for MR dampers D_1 and D_2 , respectively; the two output variables of the decentralized controller \mathbf{G}_{II} (u_3 and u_4) are the desired

optimal control forces for MR dampers D_3 and D_4 , respectively; and so on. The total number of state vectors of all three decentralized controllers, n_G , is equal to the number of state variables of the open loop system, n_{OL} , which is equal to 18 according to Eqns (4) and (5). Following Eqns (9) and (10), n_G is evenly distributed to each decentralized controller, i.e. each decentralized controller has six state variables for case DC2. Similarly, the dimensions of the decentralized controllers for cases DC1, DC3 and DC4 can be obtained as shown in Table 1.

In the wireless control implementation, one decentralized controller in the formulation may be realized through multiple wireless units. Again considering case DC2 as an example, the decentralized controller \mathbf{G}_I is implemented using wireless units \mathbf{C}_1 and \mathbf{C}_2 , \mathbf{G}_{II} is implemented using wireless units \mathbf{C}_3 and \mathbf{C}_4 , and so on. The computing associated with decentralized controller \mathbf{G}_I at every time step includes Eqns. (10a) and (10b). To allow each wireless unit keep its own copy of the state vector \mathbf{x}_{G_I} , both wireless units \mathbf{C}_1 and \mathbf{C}_2 conduct the complete calculation in Eqn (10a). In addition, since each wireless unit determines the optimal control force for only one MR damper, the unit needs to conduct calculation corresponding to only one row of Eqn (10b).

3.3. Communication and Timing

Figure 5 illustrates the communication sequences at each sampling time step for four control architectures. For case DC1, each wireless unit does not need data from other units for control decisions, therefore, no wireless transmission is required for case DC1. Since the wireless transmission of a single data packet takes about 1.5ms to 2ms for the Narada units, considering case DC2, approximately 4ms are needed at every time step for the two wireless units in each channel to transmit sensor data. For case DC2, at the 2ms of each time step, wireless units \mathbf{C}_1 , \mathbf{C}_3 , and \mathbf{C}_5 each simultaneously broadcasts its directly measured inter-story velocity data, using three different wireless frequency channels (subnets). Upon receiving the data, wireless units \mathbf{C}_2 , \mathbf{C}_4 , and \mathbf{C}_6 each broadcasts their inter-story data at the 4ms, and the wireless communication ends at the 6ms. To conduct the wireless communication, the ATmega128

microcontroller of each wireless unit only needs to send and receive data from the associated Chipcon CC2420 modem; the modem then handles the actual transmission of the data packets. Since the data exchange between the microcontroller and the modem is completed through the fast onboard SPI (Serial Peripheral Interface) port, the microcontroller only spends less than 0.1ms for every sending or receiving action. This allows the microcontroller to be dedicated for the embedded computing tasks.

Similarly, for case DC3, simultaneous wireless communication is performed using two wireless channels, and the wireless communication takes 6ms in total (starting at the 2ms and ending at the 8ms). For case DC4, only one wireless channel is used, and each wireless unit broadcasts its sensor data sequentially. During the experiments, very little interference among different wireless channels has been observed when multiple channels operate simultaneously. In our experiments, a maximum of three wireless channels operate simultaneously (DC2). In fact, the Chipcon CC2420 modem may support the simultaneous operation of up to sixteen wireless channels. Following the IEEE 802.15.4 standard, these sixteen channels are allocated within the 2.4 GHz band, in 5 MHz steps (Chipcon 2008).

The control sampling time step for each control architecture is determined by the wireless communication and required embedded computation. The computational procedures performed by a wireless unit include updating the damper hysteresis model (Lu, *et al.* 2008), calculating the desired control force for the MR damper, and determining appropriate command signal for the damper. In this study, the computational time constitutes the dominant part of the feedback time delay, and the time delay is approximated as one sampling time step ΔT (in accordance with Eqn (3)). Different decentralized architectures require different computational demand on the wireless unit, which leads to different time delays as shown in Figure 5, i.e. 7ms for DC1, 12ms for DC2, etc. At the end of the embedded computing of each sampling time step, 1ms of cushion time is allocated to ensure reliability. Due to the large amount of computation required by DC4 (e.g. larger matrices and vectors are involved in the computation described by Eqn (10a)), the centralized case DC4 has the longest time delay (i.e. sampling time step) of 47ms.

3.4. Performance of Wireless Decentralized \mathcal{H}_∞ Feedback Control

The 1940 El Centro NS (Imperial Valley Irrigation District Station) earthquake excitation with the peak ground acceleration (PGA) scaled to 1m/s^2 is employed in this study. Figure 6 shows the inter-story velocity data, $v_4 - v_3$, which is collected by three wireless units during a shake table test for decentralized control case DC3. The figure also plots the same data collected by the baseline cabled DAQ system. During the test, the inter-story velocity is measured by wireless unit C_4 at every sampling time step, and then immediately broadcasted to units C_5 and C_6 that share the same wireless channel (subnet). After the test, the inter-story velocity histories stored in all three units were transmitted to a computer for later analysis. Close agreement among the four data sets in Figure 6 demonstrates the reliability of real-time sensing feedback through simultaneous communication using multiple wireless channels (subnets).

Again considering the experimental test for case DC3 as an example, Figure 7 plots the desired force u_4 (for damper D_4) during the earthquake excitation. The force history from wireless unit C_4 is calculated onboard by the ATmega128 microcontroller, as a realization to the decentralized controller \mathbf{G}_H for the DC3 case shown in Figure 4. After the test run, all sensor data are collected on a computer and a Matlab program is written to re-enact the online computing that occurred in wireless unit C_4 . The close match between these two data sets reveals the high accuracy achieved by the embedded real-time control software.

At every control sampling time step, after the desired control force for MR damper D_4 is calculated by wireless unit C_4 , the unit immediately evaluates the current hysteretic status of the MR damper. The wireless unit then issues a damper command voltage so that the damper delivers a control force as close as possible to the desired force. Figure 8 plots the damper command voltage computed online by wireless unit C_4 , as well as the actual command voltage delivered to damper D_4 and measured by the cabled DAQ system. For clarity, the figure is zoomed in to two seconds during the test run for case DC3. Close agreement between these two sets of voltages is observed. The results show that after determining damper

command voltage, the control signal generation module of unit C_4 is capable of generating and delivering the signal to the MR damper D_4 .

Besides the experiments, numerical simulations are conducted for different control architectures using the scaled El Centro ground excitation. Figure 9(a) shows the simulated peak inter-story drifts for different control architectures during the ground excitation, as well as the simulated peak drifts of two passive control cases, where the damper command voltages are fixed to the maximum (0.8V) and minimum (0V) values, respectively. Among all the passive and feedback control cases, the simulation results indicate that feedback control case DC3 achieves the most uniform peak inter-story drifts among the six stories. In addition, the three decentralized feedback control cases (DC1, DC2, and DC3) generally outperform the centralized case DC4 and the passive cases, in terms of achieving uniformly less peak drifts.

Figure 9(b) presents the experimental peak inter-story drifts for the two passive and four feedback control cases. Although the experimental peak drift values are somewhat different from the simulated values, the results are of reasonable agreement. Figure 9(b) shows during the experiments, the \mathcal{H}_∞ control through real-time wireless sensing feedback can achieve better performance than the passive control cases (with damper command voltages set to 0.8V or 0V). For this set of experiments, the centralized case DC4 achieves slightly better control performance than the decentralized case DC3, which is different from the simulated results. Such slight difference could well be attributed to the structure and damper model uncertainties, which could have adverse effects to the experimental control performance and need further investigations. More importantly, both the simulations and experiments demonstrate that decentralized wireless feedback control can outperform passive control in terms of reducing peak inter-story drifts.

In addition to peak inter-story drifts, Figure 10 presents the root-of-mean-square (RMS) values of the inter-story drifts to reflect the control performance over the complete time history. The RMS drifts demonstrate similar trend as the peak drifts shown in Figure 9. As compared with passive control cases,

the feedback control architectures can achieve reduction to inter-story drifts over the complete time history. Furthermore, both simulation and experimental results reveal that for decentralized control, it is important to balance between minimizing time delays and the availability of sensor measurement data for control decisions. On the one hand, having more sensor data available can be beneficial for making more informed control decisions; on the other hand, the requirement for more sensor data may cause longer computation and communication latency that is disadvantageous for control performance.

4. SUMMARY AND DISCUSSION

This paper presents an experimental study for a time-delayed decentralized \mathcal{H}_∞ structural control design using homotopic transformation through linear matrix inequalities. Real-time feedback time delay, which may include communication or computing delay, is especially considered in the control formulation. Simultaneous wireless communication within multiple wireless subnets has been successfully implemented for the decentralized feedback control of a six-story scaled structure instrumented with magnetorheological dampers. Both simulation and experimental results demonstrate that the decentralized \mathcal{H}_∞ structural control approach using wireless sensing and embedded computing are viable and can outperform passive controls. The results also illustrate that to achieve optimal control performance, the minimization of feedback time delays needs to be carefully balanced against the availability of sensor measurement data.

For the decentralized control approaches adopted in this study, current implementation of wireless sensor data feedback does not allow communication between different subnets. Future investigation may explore implementation that allows inter-subnet communication to achieve information overlapping between multiple control groups. Such overlapping is expected to improve control performance by increasing sensor data availability. In addition, the feedback time delay in the current wireless control system is mostly caused by the floating-point number operations using the 8-bit ATmega128 microcontroller. Future investigation may adopt faster embedded hardware that can minimize computational time delay.

5. ACKNOWLEDGEMENTS

This work was partially supported by NSF, Grant Number CMMI-0824977, awarded to Prof. Kincho H. Law of Stanford University. The authors would like to thank Prof. Chin-Hsiung Loh and Mr. Kung-Chun Lu of the National Taiwan University, as well as Dr. Pei-Yang Lin of NCREC, for their generous assistance with the shake-table experiments. The authors also appreciate the help with the Narada wireless units from Prof. Jerome P. Lynch, Mr. R. Andrew Swartz, and Mr. Andrew T. Zimmerman of the University of Michigan. Any opinions, findings and conclusions expressed in this paper are those of the authors and do not necessarily reflect the views of their collaborators and the National Science Foundation.

REFERENCES

- Balandin, D.V. and Kogan, M.M. (2005). "LMI-based optimal attenuation of multi-storey building oscillations under seismic excitations," *Structural Control and Health Monitoring*, Vol. 12, No. 2, pp. 213-224.
- Çelebi, M. (2002). *Seismic Instrumentation of Buildings (with Emphasis on Federal Buildings)*. Report No. 0-7460-68170, United States Geological Survey, Menlo Park, CA.
- Chase, J.G., Smith, H.A. and Suzuki, T. (1996). "Robust H_∞ control considering actuator saturation. II: applications," *Journal of Engineering Mechanics*, Vol. 122, No. 10, pp. 984-993.
- Chiang, R.Y. and Safonov, M.G. (1998). *MATLAB robust control toolbox*, MathWorks, Inc., Natick, MA.
- Texas Instruments Norway AS (2008). *2.4 GHz IEEE 802.15.4 / ZigBee-ready RF Transceiver*. Oslo, Norway.
- Gahinet, P. and Apkarian, P. (1994). "A linear matrix inequality approach to H_∞ control," *International Journal of Robust and Nonlinear Control*, Vol. 4, No. 4, pp. 421-448.
- Housner, G.W., Bergman, L.A., Caughey, T.K., Chassiakos, A.G., Claus, R.O., Masri, S.F., Skelton, R.E., Soong, T.T., Spencer, B.F., Jr. and Yao, J.T.P. (1997). "Structural control: past, present, and future," *Journal of Engineering Mechanics*, Vol. 123, No. 9, pp. 897-971.

- Johnson, E.A., Voulgaris, P.G. and Bergman, L.A. (1998). "Multiobjective optimal structural control of the Notre Dame building model benchmark," *Earthquake Engineering & Structural Dynamics*, Vol. 27, No. 11, pp. 1165-1187.
- Kurino, H., Tagami, J., Shimizu, K. and Kobori, T. (2003). "Switching oil damper with built-in controller for structural control," *Journal of Structural Engineering*, Vol. 129, No. 7, pp. 895-904.
- Lin, C.-C., Chang, C.-C. and Chen, H.-L. (2006). "Optimal H_∞ output feedback control systems with time delay," *Journal of Engineering Mechanics*, Vol. 132, No. 10, pp. 1096-1105.
- Lu, K.-C., Loh, C.-H., Yang, J.N. and Lin, P.-Y. (2008). "Decentralized sliding mode control of a building using MR dampers," *Smart Materials and Structures*, Vol. 17, No. 5, pp. 055006.
- Lunze, J. (1992). *Feedback Control of Large Scale Systems*, Prentice-Hall, Englewood Cliffs, NJ.
- Lynch, J.P., Wang, Y., Lu, K.-C., Hou, T.-C. and Loh, C.-H. (2006). "Post-seismic damage assessment of steel structures instrumented with self-interrogating wireless sensors," *Proceedings of the 8th National Conference on Earthquake Engineering*, San Francisco, CA, April 18 - 21.
- Mahmoud, M.S., Terro, M.J. and Abdel-Rohman, M. (1998). "An LMI approach to H_∞ -control of time-delay systems for the benchmark problem," *Earthquake Engineering & Structural Dynamics*, Vol. 27, No. 9, pp. 957-976.
- Mehendale, C.S. and Grigoriadis, K.M. (2008). "A double homotopy method for decentralised control design," *International Journal of Control*, Vol. 81, No. 10, pp. 1600 - 1608.
- Sandell, N., Jr., Varaiya, P., Athans, M. and Safonov, M. (1978). "Survey of decentralized control methods for large scale systems," *Automatic Control, IEEE Transactions on*, Vol. 23, No. 2, pp. 108-128.
- Shimizu, K., Yamada, T., Tagami, J. and Kurino, H. (2004). "Vibration tests of actual buildings with semi-active switching oil damper," *Proceedings of the 13th World Conference on Earthquake Engineering*, Vancouver, B.C., Canada, August 1 - 6.
- Siljak, D.D. (1991). *Decentralized Control of Complex Systems*, Academic Press, Boston.

- Spencer, B.F., Jr. and Nagarajaiah, S. (2003). "State of the art of structural control," *Journal of Structural Engineering*, Vol. 129, No. 7, pp. 845-856.
- Straser, E.G. and Kiremidjian, A.S. (1998). *A Modular, Wireless Damage Monitoring System for Structures*. Report No. 128, John A. Blume Earthquake Eng. Ctr., Stanford University, Stanford, CA.
- Swartz, R.A., Jung, D., Lynch, J.P., Wang, Y., Shi, D. and Flynn, M.P. (2005). "Design of a wireless sensor for scalable distributed in-network computation in a structural health monitoring system," *Proceedings of the 5th International Workshop on Structural Health Monitoring*, Stanford, CA, September 12 - 14.
- Swartz, R.A. and Lynch, J.P. (2009). "Strategic network utilization in a wireless structural control system for seismically excited structures," *Journal of Structural Engineering*, Vol. 135, No. 5, pp. 597-608.
- VanAntwerp, J.G. and Braatz, R.D. (2000). "A tutorial on linear and bilinear matrix inequalities," *Journal of Process Control*, Vol. 10, No. 4, pp. 363-385.
- Wang, S.-G. (2003). "Robust active control for uncertain structural systems with acceleration sensors," *Journal of Structural Control*, Vol. 10, No. 1, pp. 59-76.
- Wang, Y., Swartz, R.A., Lynch, J.P., Law, K.H., Lu, K.-C. and Loh, C.-H. (2007). "Decentralized civil structural control using real-time wireless sensing and embedded computing," *Smart Structures and Systems*, Vol. 3, No. 3, pp. 321-340.
- Wang, Y., Swartz, R.A., Zimmerman, A., Askin, A.C., Lynch, J.P., Law, K.H., Lu, K.-C. and Loh, C.-H. (2008). "Decentralized wireless structural sensing and control with multiple system architectures operating at different sampling frequencies," *Proceedings of SPIE, Health Monitoring of Structural and Biological Systems II*, San Diego, CA, March 9 - 13.
- Wang, Y. (2009). "Time-delayed dynamic output feedback H_∞ controller design for civil structures: a decentralized approach through homotopic transformation," *Structural Control and Health Monitoring*, Vol. <http://dx.doi.org/10.1002/stc.344>.

- Wang, Y., Law, K.H. and Lall, S. (2009). "Time-delayed decentralized H_∞ controller design for civil structures: a homotopy method through linear matrix inequalities," *Proceedings of the 2009 American Control Conference (ACC 2009)*, St. Louis, MO, USA, June 10 - 12.
- Yang, J.N., Lin, S. and Jabbari, F. (2004). " H_∞ -based control strategies for civil engineering structures," *Structural Control and Health Monitoring*, Vol. 11, No. 3, pp. 223-237.
- Zhai, G., Ikeda, M. and Fujisaki, Y. (2001). "Decentralized H_∞ controller design: a matrix inequality approach using a homotopy method," *Automatica*, Vol. 37, No. 4, pp. 565-572.
- Zhou, K., Doyle, J.C. and Glover, K. (1996). *Robust and Optimal Control*, Prentice Hall, Englewood Cliffs, NJ.

LIST OF FIGURES AND TABLES

Figure 1. Diagram of the structural control system.

Figure 2. Experimental setup for \mathcal{H}_∞ feedback control using wireless sensing and control units.

Figure 3. Narada wireless sensing and control unit (Swartz, *et al.* 2005, Swartz and Lynch 2009).

Figure 4. Multiple feedback control architectures and the associated sampling time step lengths.

Figure 5. Illustration of wireless communication and embedded computing at every sampling time step for four control architectures.

Figure 6. Time history of inter-story velocity $v_4 - v_3$ during a shake table test for decentralized control case DC3.

Figure 7. Desired control force u_4 (for MR damper D_4) during a shake table test for decentralized control case DC3.

Figure 8. Command voltage for MR damper D_4 within randomly selected 2 seconds.

Figure 9. Peak inter-story drifts for El Centro ground excitation with PGA scaled to 1m/s^2 .

Figure 10. RMS inter-story drifts for El Centro ground excitation with PGA scaled to 1m/s^2 (note that the horizontal scales are different from these in Figure 9).

Table 1 Dimensions of the decentralized dynamic controllers for four control architectures.

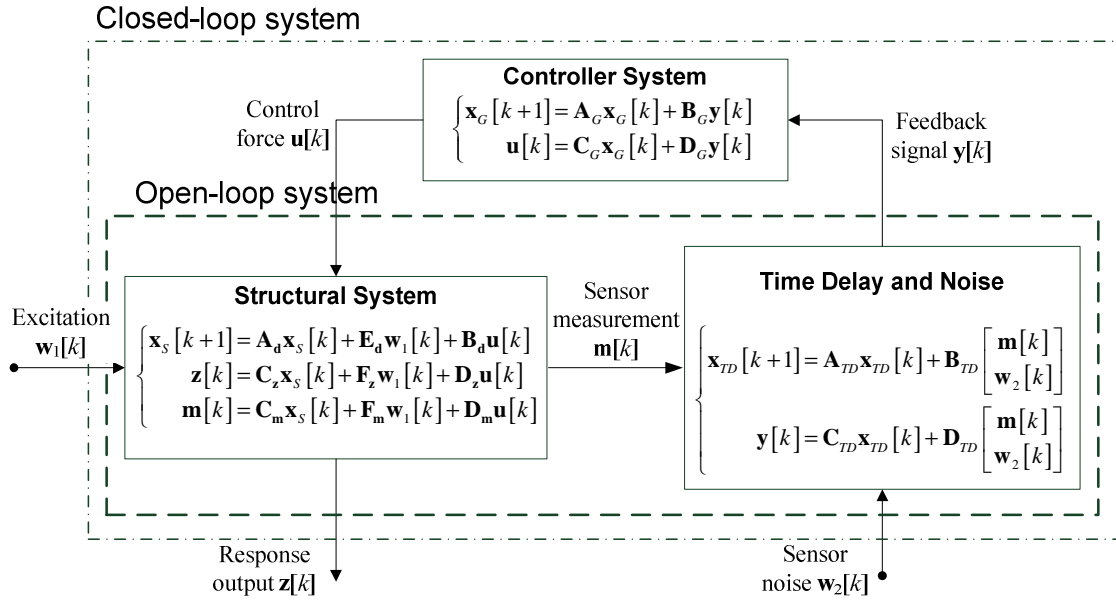
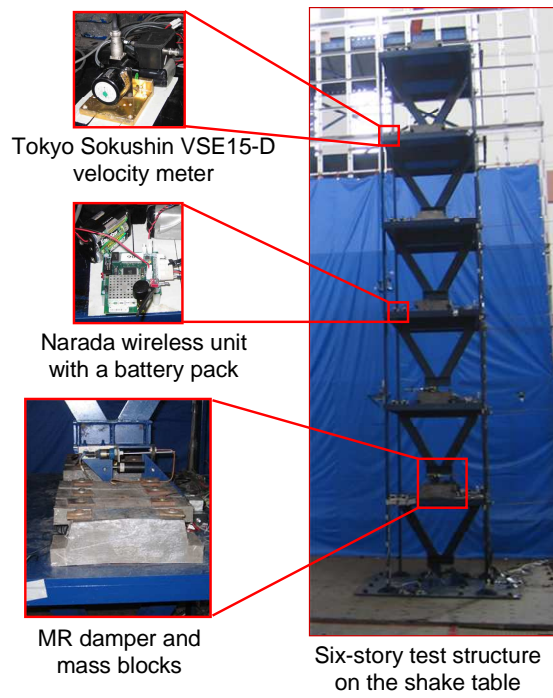


Figure 1. Diagram of the structural control system.



(a) The six-story experimental structure

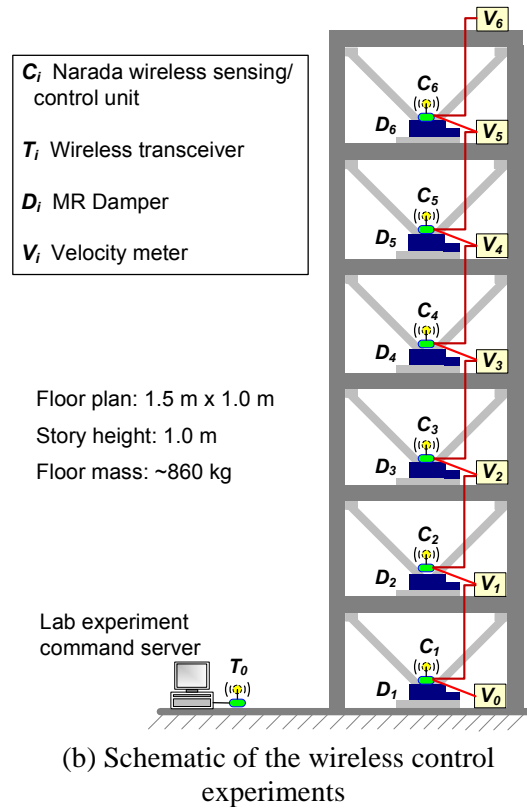


Figure 2. Experimental setup for \mathcal{H}_∞ feedback control using wireless sensing and control units.

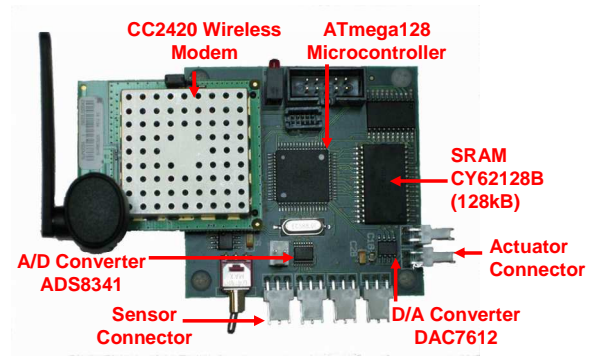


Figure 3. Narada wireless sensing and control unit (Swartz, *et al.* 2005, Swartz and Lynch 2009).

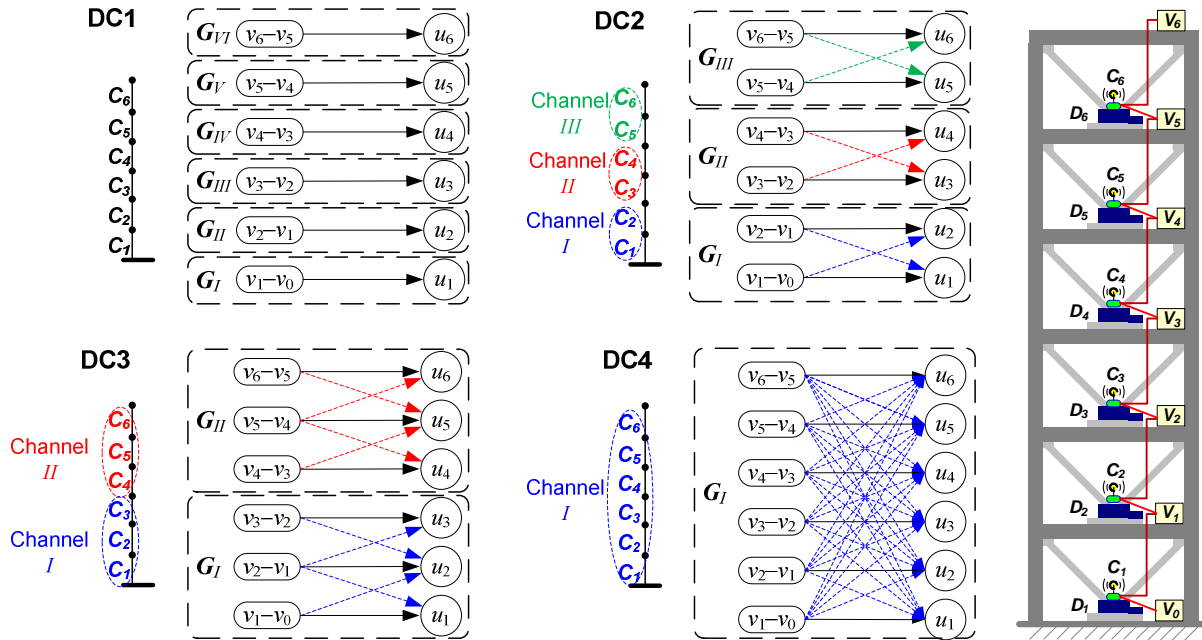


Figure 4. Multiple feedback control architectures and the associated sampling time step lengths.

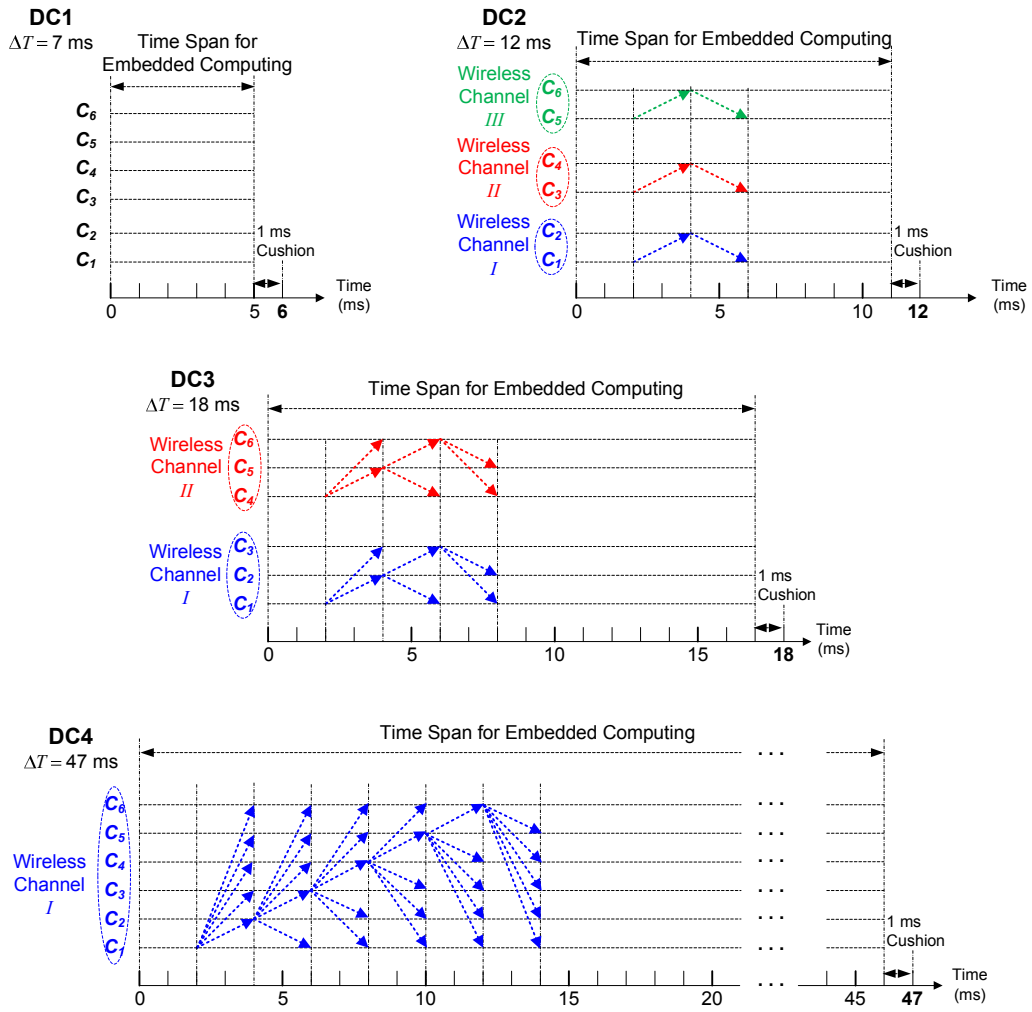


Figure 5. Illustration of wireless communication and embedded computing at every sampling time step for four control architectures.

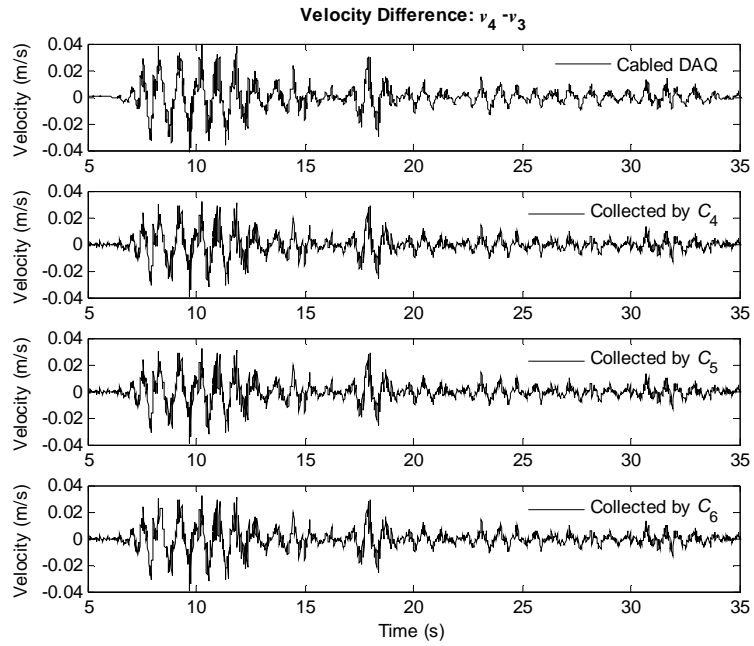


Figure 6. Time history of inter-story velocity $v_4 - v_3$ during a shake table test for decentralized control case DC3.

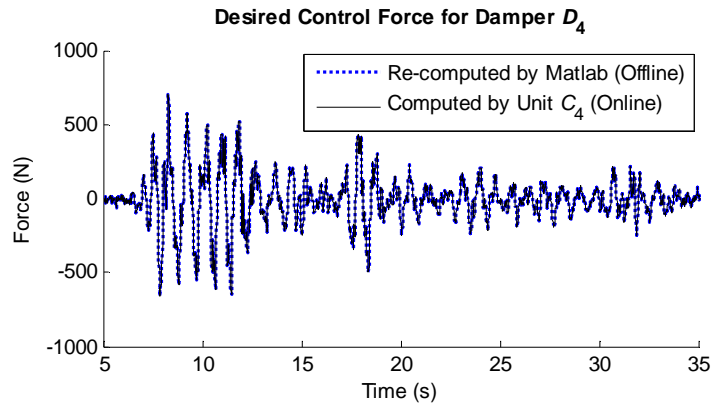


Figure 7. Desired control force u_4 (for MR damper D_4) during a shake table test for decentralized control case DC3.

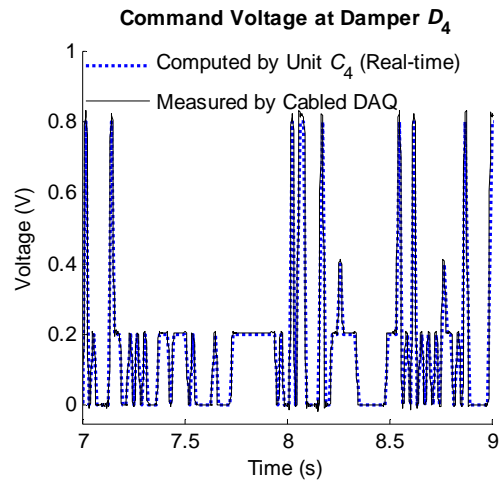
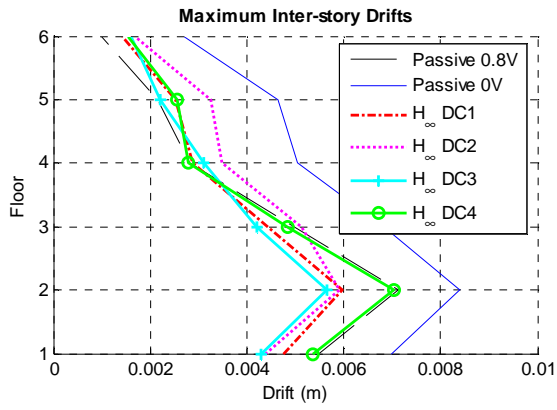
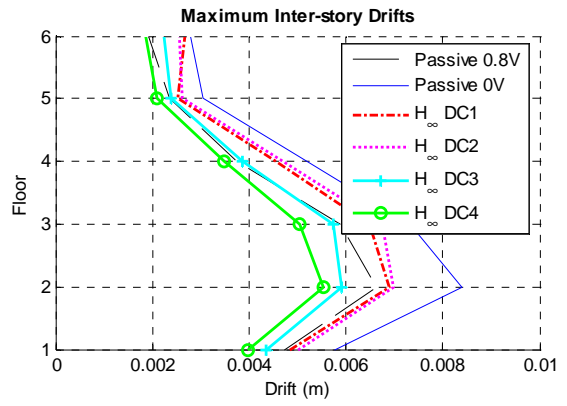


Figure 8. Command voltage for MR damper D_4 within randomly selected 2 seconds.

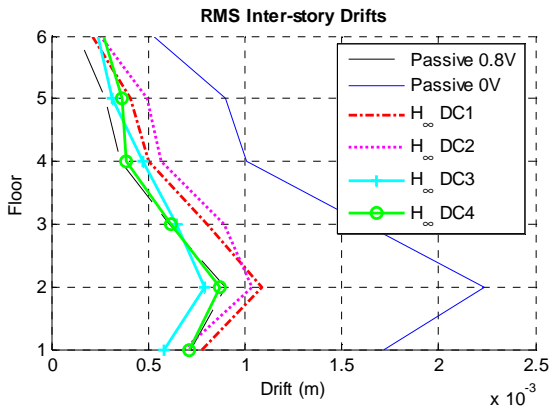


(a) Simulation results

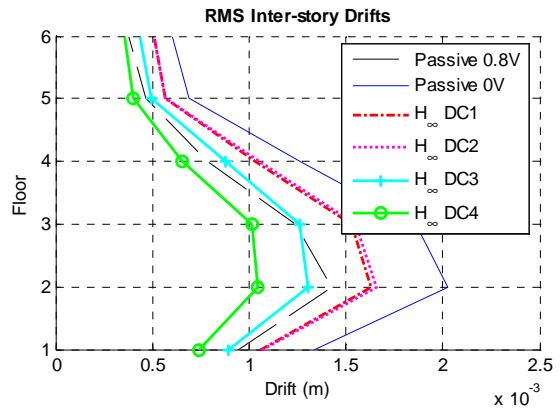


(b) Experimental results

Figure 9. Peak inter-story drifts for El Centro ground excitation with PGA scaled to 1m/s^2 .



(a) Simulation results



(b) Experimental results

Figure 10. RMS inter-story drifts for El Centro ground excitation with PGA scaled to 1m/s^2 (note that the horizontal scales are different from these in Figure 9).

Table 1 Dimensions of the decentralized dynamic controllers for four control architectures.

	DC1						DC2			DC3		DC4
	G_I	G_{II}	G_{III}	G_{IV}	G_V	G_{VI}	G_I	G_{II}	G_{III}	G_I	G_{II}	G_I
Number of Input Variables	1	1	1	1	1	1	2	2	2	3	3	6
Number of State Variables	3	3	3	3	3	3	6	6	6	9	9	18
Number of Output Variables	1	1	1	1	1	1	2	2	2	3	3	6